Dynamic rubidium-82 PET/CT as a novel tool for quantifying hemodynamic differences in renal blood flow using a one-tissue compartment model

Burgt, A. van de; Velden, F.H.P. van; Kwakkenbos, K.; Smit, F.; Geus-Oei, L.F. de; Dekkers, I.A.

Received: 30 October 2023 | Revised: 1 March 2024 | Accepted: 4 April 2024

DOI: 10.1002/mp.17080

RESEARCH ARTICLE

MEDICAL PHYSICS

Dynamic rubidium-82 PET/CT as a novel tool for quantifying hemodynamic differences in renal blood flow using a one-tissue compartment model

Alina van de Burgt[1,2] | **Floris H. P. van Velden**[2] | **Koen Kwakkenbos**[1,2] | **Frits Smit**[1,2] | **Lioe-Fee de Geus-Oei**[2,3,4] | **Ilona A. Dekkers**[2]

[1]Department of Nuclear Medicine, Alrijne hospital, Leiderdorp, The Netherlands

[2]Department of Radiology, Leiden University Medical Center, Leiden, The Netherlands

[3]Biomedical Photonic Imaging Group, University of Twente, Enschede, The Netherlands

[4]Department of Radiation Science & Technology, Delft University of Technology, Delft, The Netherlands

Correspondence
Alina van de Burgt, MSc, Department of Radiology, Section of Nuclear Medicine, Leiden University Medical Center, PO Box 9600, 2300 RC Leiden, The Netherlands.
Email: a.van_de_burgt@lumc.nl

Funding information
Dutch Science Foundation, Grant/Award Number: 09150162210040

Abstract

Purpose: Assessing renal perfusion in-vivo is challenging and quantitative information regarding renal hemodynamics is hardly incorporated in medical decision-making while abnormal renal hemodynamics might play a crucial role in the onset and progression of renal disease. Combining physiological stimuli with rubidium-82 positron emission tomography/computed tomography (^{82}Rb PET/CT) offers opportunities to test the kidney perfusion under various conditions. The aim of this study is: (1) to investigate the application of a one-tissue compartment model for measuring renal hemodynamics with dynamic ^{82}Rb PET/CT imaging, and (2) to evaluate whether dynamic PET/CT is sensitive to detect differences in renal hemodynamics in stress conditions compared to resting state.

Methods: A one-tissue compartment model for the kidney was applied to cardiac ^{82}Rb PET/CT scans that were obtained for ischemia detection as part of clinical care. Retrospective data, collected from 17 patients undergoing dynamic myocardial ^{82}Rb PET/CT imaging in rest, were used to evaluate various CT-based volumes of interest (VOIs) of the kidney. Subsequently, retrospective data, collected from 10 patients (five impaired kidney functions and five controls) undergoing dynamic myocardial ^{82}Rb PET/CT imaging, were used to evaluate image-derived input functions (IDIFs), PET-based VOIs of the kidney, extraction fractions, and whether dynamic ^{82}Rb PET/CT can measure renal hemodynamics differences using the renal blood flow (RBF) values in rest and after exposure to adenosine pharmacological stress.

Results: The delivery rate (K_1) values showed no significant ($p = 0.14$) difference between the mean standard deviation (SD) K_1 values using one CT-based VOI and the use of two, three, and four CT-based VOIs, respectively 2.01(0.32), 1.90(0.40), 1.93(0.39), and 1.94(0.40) mL/min/mL. The ratio between RBF in rest and RBF in pharmacological stress for the controls were overall significantly lower compared to the impaired kidney function group for both PET-based delineation methods (region growing and iso-contouring), with the smallest median interquartile range (IQR) of 0.40(0.28–0.66) and 0.96(0.62–1.15), respectively ($p < 0.05$). The K_1 of the impaired kidney function group were close to 1.0 mL/min/mL.

Conclusions: This study demonstrated that obtaining renal K_1 and RBF values using ^{82}Rb PET/CT was feasible using a one-tissue compartment model. Applying iso-contouring as the PET-based VOI of the kidney and using AA as an IDIF is suggested for consideration in further studies. Dynamic ^{82}Rb PET/CT imaging showed significant differences in renal hemodynamics in rest compared to when exposed to adenosine. This indicates that dynamic ^{82}Rb PET/CT has potential to detect differences in renal hemodynamics in stress conditions compared to the resting state, and might be useful as a novel diagnostic tool for assessing renal perfusion.

KEYWORDS
82Rb PET/CT, dynamic rubidium-82 PET/CT, one-tissue compartment model, renal blood flow, renal hemodynamics, renal perfusion

1 | INTRODUCTION

The prevalence of chronic kidney disease (CKD) is projected to substantially increase upcoming decades, requiring new strategies for earlier diagnosis.[1,2] The human kidney receives ca. 20% of cardiac output and disturbances in renal blood flow (RBF) might play a major role in CKD.[3] However, evaluation of renal macro- and microcirculation is currently unused, since validated non-invasive methods for assessing kidney perfusion are lacking.

Imaging has important benefits for determining renal perfusion compared to time-honored gold standard methods such as para-aminohippurate clearance; it is less invasive, faster and allows for regional comparison within the kidney and between the kidneys.[3–6] [^{15}O]H_2O positron emission tomography/computed tomography (PET/CT) is a widely used technique to assess renal perfusion.[3] However, rubidium-82 (^{82}Rb) PET/CT might be an alternative technique, which is easy to implement as it does not require an on-site cyclotron.

^{82}Rb PET/CT is increasingly being used for cardiac perfusion imaging. The flow tracer ^{82}Rb accumulates in the cells, has a short physical half-life (75 s) and a high first-pass extraction in the kidneys that also enables renal perfusion quantification, but is not yet used for this application in clinical practice. From renal physiology studies it is known that kidney function increases after a stimulus such as an oral protein load or an intravenous infusion with amino acids, glucagon, or dopamine.[5] Combining physiological stimuli with ^{82}Rb PET/CT offers unique opportunities to test the kidney under various conditions making dynamic ^{82}Rb PET/CT an interesting technique for dedicated renal stress testing.[6–9]

One-tissue compartment models have been validated for myocardial blood flow quantification and are currently in routine clinical use.[10,11] Previous work by Tahari et al. and Langaa et al. demonstrated the feasibility of ^{82}Rb PET/CT with one-tissue compartment models for assessing renal perfusion.[12,13] However, there is no uniform approach regarding kidney compartment modeling and hence further research is necessary to investigate the effect of various inputs, outputs, and extraction fractions on the RBFs to enable evaluation of disease activity and treatment response monitoring. Therefore, the aim of this study is: (1) to investigate the application of a one-tissue compartment model for measuring renal hemodynamics with dynamic ^{82}Rb PET/CT imaging, and (2) to evaluate whether dynamic PET/CT is sensitive to detect differences in renal hemodynamics in stress conditions compared to resting state.

2 | METHODS

2.1 | Study design

This was a retrospective proof-of-concept study and a waiver was obtained by the medical ethical review board to perform this study. Written informed consent was obtained from all participants. Clinical characteristics were collected from patient records and the ^{82}Rb PET/CT reports.

2.2 | Population

Patients coming for a myocardial perfusion ^{82}Rb PET/CT in the period between March 2020 and November 2022 were retrospectively selected based on the amount of kidney tissue in the field of view (FoV). At least 5.7 cm (15 consecutive CT slices) of the most superior kidney on the CT data was required to perform the analysis.

Two different patient datasets were used in this study: (A) dynamic rest myocardial ^{82}Rb PET/CT data ($N = 17$) were used to evaluate various manual CT-based volume of interest (VOI) methods of the kidney with one-tissue compartment models to district between the cortex and the medulla. Subsequently, (B) dynamic myocardial rest and pharmacological stress ^{82}Rb PET/CT data with adenosine were selected to illustrate the effects of

various semi-automatic PET-based kidney delineations, image derived input functions (IDIFs) and extraction fractions to convert the delivery rate (K_1) values to flow values, and to assess the resulting differences in renal hemodynamics in stress conditions compared to resting state with ^{82}Rb PET/CT imaging ($N = 10$, five impaired kidney functions and five controls). The five subjects with impaired kidney function were selected based on an eGFR < 60 mL/min/1.73 m^2.[14] As comparison five subjects (considered as controls) without history of cardiovascular disease or interventions, calcium score 0, MFR > 1.5, no cardiac perfusion defects, chronic obstructive pulmonary disease (COPD), lung emphysema, malignancies other than T1 locally resected, diabetes mellitus type 1 (DM1), or type 2 (DM2) were selected.

2.3 | Data collection

PET/CT images were obtained on a Discovery MI 5-Ring PET/CT (GE Healthcare, Chicago, Illinois, USA). A low dose CT (20 mAs, 120 kV) was acquired for attenuation correction purposes and reconstructed in a 512 by 512 matrix and an FoV of 70 cm (with a voxel size of $1.4 \times 1.4 \times 3.75$ mm^3).

PET data were acquired during a period of 6 min, starting 8 s after the automatic intravenous infusion of a bolus of approximately 750 MBq ^{82}RbCl (^{82}Sr/^{82}Rb generator, Rubigen B.V., 's Hertogenbosch, The Netherlands) in a resting state (referred to rest acquisition). Subsequently, a second acquisition was started following the same protocol with similar activity 2.5 min after an adenosine infusion (140 µg/kg/min over 6 min) (referred to as the stress acquisition).

PET data were acquired in list mode and reconstructed in multiple time frames using a time-of-flight ordered subset expectation maximization algorithm (VPFX TOF-OSEM; 2 subsets, 17 iterations) on a 128 by 128 matrix (with a voxel size of $2.8 \times 2.8 \times 2.8$ mm^3) with a 5.0 mm full-width-at-half maximum (FWHM) Hanning filter. A total of 26 time frames were reconstructed per PET scan, that is, 10×5, 6×10, 5×15, and finally 5×20 s. Images were normalized and corrected for radioactive decay, attenuation, and scatter.

2.4 | Kinetic modeling

An existing one-tissue compartment model was used to calculate global K_1 values based on renal one-tissue compartment models from previous studies,[12,13] as depicted in Figure 1.

PMOD software package (version 4.2; PMOD Technologies Ltd., Zurich, Switzerland) was used for kinetic modeling. Equation (1) shows the change in ^{82}Rb concentration in the kidney compartment:

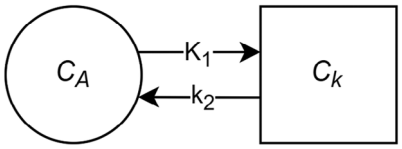

FIGURE 1 A visual representation of a one-tissue compartment model: C_A, vascular compartment; C_k, tissue compartment; K_1, uptake rate of rubidium-82 from the vascular compartment to the tissue compartment; k_2, fraction of rubidium-82 from the tissue compartment to the vascular compartment.

$$\frac{dC_k(t)}{dt} = K_1 C_A(t) - k_2 C_k(t) \quad (1)$$

In this equation, the rate constant K_1 denotes the perfusion-dependent component and has unit mL/min/mL. The rate constant k_2 indicates the rate in which the ^{82}Rb leaves the kidney parenchyma and has unit min^{-1}. Furthermore, the functions C_A and C_k represent the concentration (kBq/mL) per timepoint in the vascular input and the kidney parenchyma, respectively. For the input C_A in Equation (3), we used an IDIF, as no blood samples were drawn from patients during scanning. Equation (1) can be analytically solved, yielding:

$$C_k(t) = K_1 \int_0^t C_A(t)\, e^{-k_2(t-\tau)} d\tau \quad (2)$$

Which can be expressed as a convolution:

$$C_k(t) = K_1 e^{-k_2 t} * C_A(t) \quad (3)$$

Finally, an operational model curve is fitted by PMOD, considering the blood volume fraction (v_B):

$$C_{\text{model}} = (1 - v_B)\, C_k(t) + v_B C_A(t) \quad (4)$$

A constant value of 0.10 for v_B was used to account for activity from the fractional blood volume within the VOI, as previously used by Langaa et al.[13,15] The rate constants K_1 and k_2 were estimated in PMOD by means of a least-squares method in an iterative manner, with a maximum of 20 random iterations. This was done by curve fitting which started with establishing a set of initial parameter values, from which the corresponding model curve was generated. Subsequently, the Chi-square criterion was computed, prompting adjustments to the model parameters with the goal of reducing Chi-square. Multiple fitting iterations were performed, and the result parameters were selected from the fit with the minimal chi-squared value. In this context, randomness entailed that fitting began

with randomized sets of initial parameters, utilizing a uniform distribution within a ±100% range. This intentional introduction of randomness served the purpose of preventing convergence into local minima.[16] In preliminary experiments (data not shown), this number of iterations was found to be sufficient for PMOD to find a stable minimum.

Accurate measurement of the time base of the input signal is crucial for flow tracers with high first-pass extraction as [^{15}O]H_2O and likely ^{82}Rb. Therefore, in line with existing literature, correction for delay and dispersion in the blood signal is essential.[17–19] The operational Equations (1)–(4) provided above require modification to accommodate these factors. Equation (5) represents the relationship between measured and actual arterial concentration time courses.

$$\frac{dC_A^*(t)}{dt} = \frac{1}{\tau_d}\left(C_A(t-\Delta t) - C_A^*(t)\right) \quad (5)$$

In this equation, C^*_A represents the measured arterial concentration (kBq/mL) per timepoint in the vascular input and C_A is the true arterial concentration. The delay in units of time is represented as Δt and τ_d is the dispersion constant in units of min. Solving and substituting this equation into the prior operational Equations (1)–(4) allows fitting for delay and dispersion. The correction of delay was performed in PMOD by fitting the delay together with the kinetic parameters of the tissue model.[16] The lower limit was fixed at 0, as kidney uptake cannot occur before the ^{82}Rb bolus injection. The correction for dispersion could be incorporated into the one-tissue compartment model and solved using the Laplace transform to yield the Equation (4), as described by Meyer.[20]

2.5 | Various kidney VOI delineation methods

2.5.1 | Manual delineations on CT

Using the rest dynamic ^{82}Rb PET/CT scans from dataset A (N = 17), various manual kidney VOI delineations on CT were evaluated to assess K_1 values of a combination of different parts of the kidney. VOIs were placed in the upper pole of the left kidney on an axial view of CT scan. CT-based delineation was applied with one fixed sphere (radius of 10 mm) for one VOI and two, three, or four fixed cuboids (5 mm × 10 mm × 10 mm) between the medulla and the cortex for multiple VOIs. In case two, three, or four cuboids were placed in the kidney, the first VOI was placed medial (two voxels from the right of the calyx). The second VOI was placed on the same CT slice, but two voxels from the lateral kidney boundary. Subsequently, the remainder third and fourth cuboids were set between the first and second cuboids. Finally, VOI translation from CT to PET data was executed, as depicted in Figure S1.

Effects of spill-over and partial volume were minimized by placement of the VOIs at least two voxels away from kidney boundary walls. The renal pelvis was not included in the VOI. The VOIs were not placed in the three most superior and inferior slides of the FoV, as these slides could have a slightly reduced spatial resolution as compared with more central slides of the FoV.[21] The position of the VOIs was checked for patient motion in every frame and slice.

2.5.2 | Semi-automatic PET-based delineations

Because CT contrast agents are not clinically used in myocardial ^{82}Rb PET/CT imaging for the detection of ischemia, two other semi-automatic kidney delineation methods on PET were also explored using pharmacological stress data (dataset B, N = 10), being (1) hot contouring with manual placement of a seed point and (2) an iso-contouring delineation method, only requiring the placement of a bounding box and a percentage. For the iso-contouring delineation method, a kidney VOI was placed in the average of the rest scan over time, as described in previous studies for VOI delineation of the left ventricle wall[11] and the carotid arteries.[22] In this study, a bounding box was placed around the kidney volume, after which the iso-contour was automatically generated representing 40% of the maximum within the bounding box. The region growing method required the manual identification of a temporal frame showing high signal in the entire kidney volume and placing a seed point. These delineations were repeated in order to assess the intraobserver variability for establishing the RBF in rest and stress.

2.5.3 | Image-derived input functions

A 3D sphere with a radius of 10 mm was placed in the left ventricular blood pool (LVBP) and ascending thoracic aorta (ATA) and a 3D sphere with a radius of 5 mm was placed in the abdominal aorta (AA). VOIs were placed as centrally as possible in the vessels and the ventricle, avoiding delineation of the walls, to minimize partial volume effects and spill over, respectively. An overview of the IDIF delineations is depicted in Figure S1.

After the placement of IDIFs and VOIs, time-activity curves (TACs) were generated depicting the mean activity concentrations in kBq/mL of ^{82}Rb per region over time (s) (Figure 2).

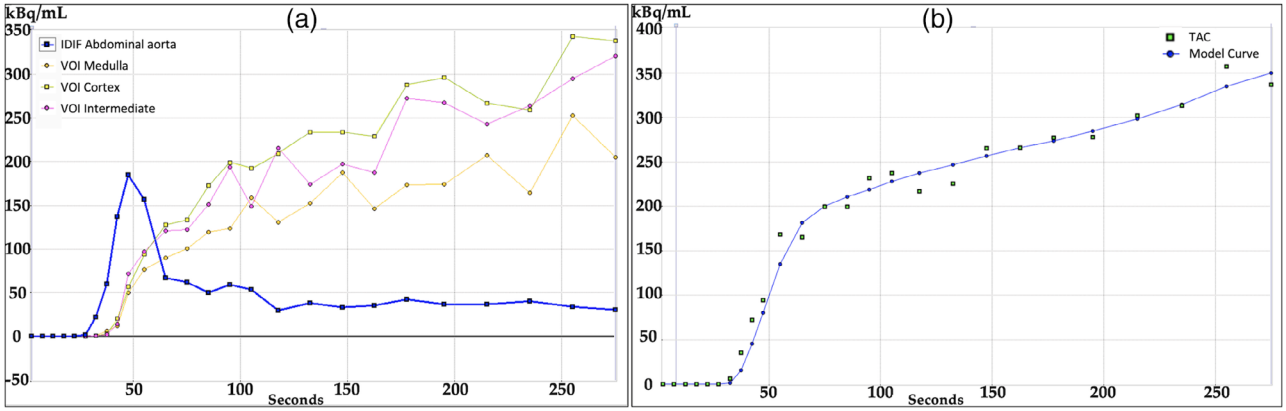

FIGURE 2 Time activity curves (TAC) after applying a volume of interest (VOI) of kidney tissue using the abdominal aorta as image derived input function. (a) Unfitted time-activity curves of three VOIs. (b) Fitted TAC of one of the kidney tissue VOIs. VOI delineations on computed tomography (CT) were applied between the medulla and the cortex.

2.6 | Renal blood flow and renovascular reserve

K_1 is a product of flow (F) and the extraction factor (E) as calculated by Equation (6):

$$K_1 = F \cdot E \tag{6}$$

The extraction factor can either be a constant value or derived from a Renkin–Crone function.[23,24] The latter is given in Equation (7), and is thought to be flow-dependent for ^{82}Rb:

$$K_1 = F \cdot \left(1 - a \cdot e^{-b/F}\right) \tag{7}$$

To convert the K_1 values to flow values, two approaches were evaluated:

(i) assuming a constant extraction fraction of 0.9 as determined in canine experiments,[7]
(ii) using the values found by Gregg et al.[25] for the kidney: $a = 0.94$ and $b = 1.86$.

All flow values were converted to mL/min/g by assuming a kidney density of 1.04 g/mL.[26,27]

Research suggests that a state of net vasodilation also occurs in kidney vasculature, but can be preceded by vasoconstriction of the afferent arterioles.[28,29] We assume that an increase in renal functioning when exposed to a stimulus (stress) is accompanied by an increase in RBF, and that the ratio compared to when such a stimulus is not present (rest) can be used for the measurement of renal hemodynamics. In this study, we refer to this ratio of RBF during exposure to adenosine (stress) compared to rest as the renovascular reserve (RVR). The RVR is calculated using Equation (8). This new parameter is similar to the coronary flow reserve used in clinical practice for assessing conditions affecting the coronary arteries.

$$\text{Renovascular reserve} = \frac{\text{RBF}_{\text{stress}}}{\text{RBF}_{\text{rest}}} \tag{8}$$

2.7 | Statistical analysis

A Shapiro–Wilk test was performed to evaluate the (log)normality of the data. The statistical analyses of the non-paired data were performed with an independent T test or Mann–Whitney U depending on the (log)normality. Continuous data were expressed as mean standard deviation (SD) or median interquartile range (IQR) depending on (log)normality. Paired data were statistically performed with the paired T-test or Wilcoxon Signed Rank test depending on the (log)normality. A one-way repeated measures analysis of variance (ANOVA) was performed to compare the total K_1 values between the number of kidney VOIs. The RVRs and RBFs of both study arms were compared using the Wilcoxon rank-sum (Mann–Whitney U) test. A p-value <0.05 was deemed significant.

Bland–Altman plots were composed to assess the intraobserver variability for establishing the RVR. Statistical analysis was performed using the statistics module SciPy (version 1.9.2) of Python (version 3.11) and Graphpad Prism (version 9.3.1; GraphPad Software, San Diego, California USA).[30]

3 | RESULTS

3.1 | Evaluation of various kidney VOI delineation methods on CT

K_1 values were composed for various kidney VOIs using AA as IDIF (dataset A, $N = 17$), as depicted in Figure 3.

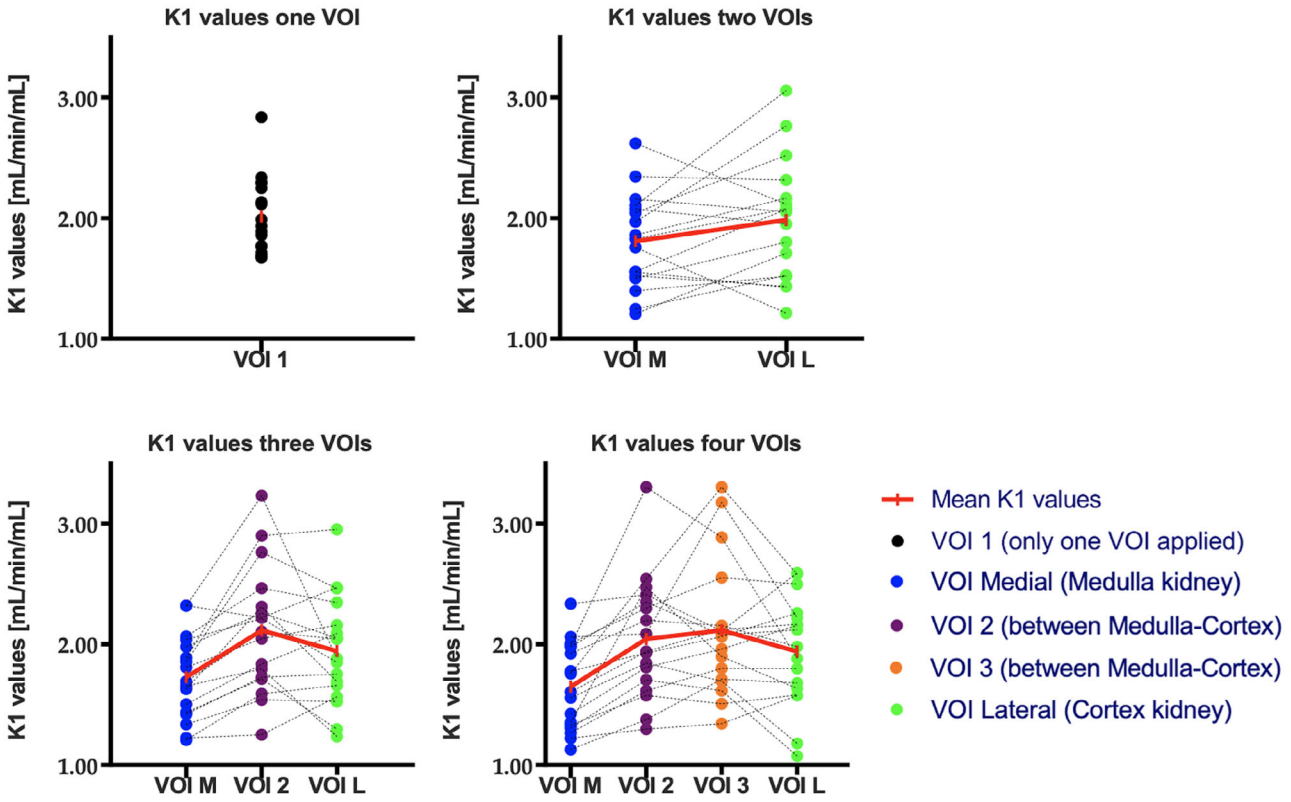

FIGURE 3 Visualization of K_1 values in mL/min/mL applying one or more volume of interest (VOI) of kidney tissue using the abdominal aorta as image derived input function ($N = 17$). Computed tomography (CT)-delineation was applied with one fixed sphere (radius of 10 mm) for one VOI and two, three, or four fixed cuboids (5 mm × 10 mm × 10 mm) between the medulla and the cortex for multiple VOIs. In case two, three, or four cuboids were placed in the kidney, the first VOI was placed medial (two voxels from the right of the calyx). The second VOI was placed on the same CT slice, but two voxels from the lateral kidney boundary. Subsequently, the remainder third and fourth cuboids were set between the first and second cuboids. Every dot represents a K_1 value of a subject ($N = 17$).

The K_1 values showed no significant ($p = 0.14$) difference between the mean (SD) K_1 values applying one VOI and the use of two, three, and four VOIs, respectively 2.01(0.32), 1.90(0.40), 1.93(0.39), and 1.94(0.40) mL/min/mL. When two VOIs were applied, no significant difference ($p = 0.10$) was found between the two VOIs in mean (SD) K_1 values, respectively 1.81(0.39) and 1.98(0.50) mL/min/mL. Furthermore, significant differences ($p < 0.05$) were identified between the VOIs of the three and four VOIs placements with mean (SD) K_1 values, respectively, 1.73(0.35), 2.12(0.52), 1.94(0.45) mL/min/mL and 1.65(0.36), 2.04(0.50), 2.12(0.56), 1.94(0.45) mL/min/mL. However, the deviation between the mean K_1 values of applying one VOI is significantly smaller ($p < 0.05$) compared to the SD applying two, three, or four VOIs (max SD of one VOI; 0.32 vs. four VOIs 0.56 mL/min/mL).

3.2 | Evaluation of renal hemodynamics

For the remainder of the study, dataset B was used for the evaluation of renal hemodynamics (Table S1). The obtained K_1 values are depicted in Figure 4 per IDIF (AA, ATA, and LVBP) and per kidney delineation method (iso-contouring and region growing). The data showed a decrease in K_1 values in stress compared to rest for controls and patients with median impaired kidney function of 20.6% and 7.9%, respectively, when iso-contouring and AA as IDIF were applied. The K_1 values of this impaired kidney function group were close to 1.0. The numeric K_1 values, k_2 values, and blood delay time per patient were reported in Table S2.

3.3 | RBF and RVR

RBF data (mL/min/g) are provided in Table S3 (rest) and Table S4 (stress). No significant differences in RBF between the control and impaired kidney group were found in stress state and in rest state ($p > 0.05$). Furthermore, no significant differences between the two kidney delineations methods for both the rest and stress were found with regards to flow values ($p > 0.05$). For the rest phase, no significant differences

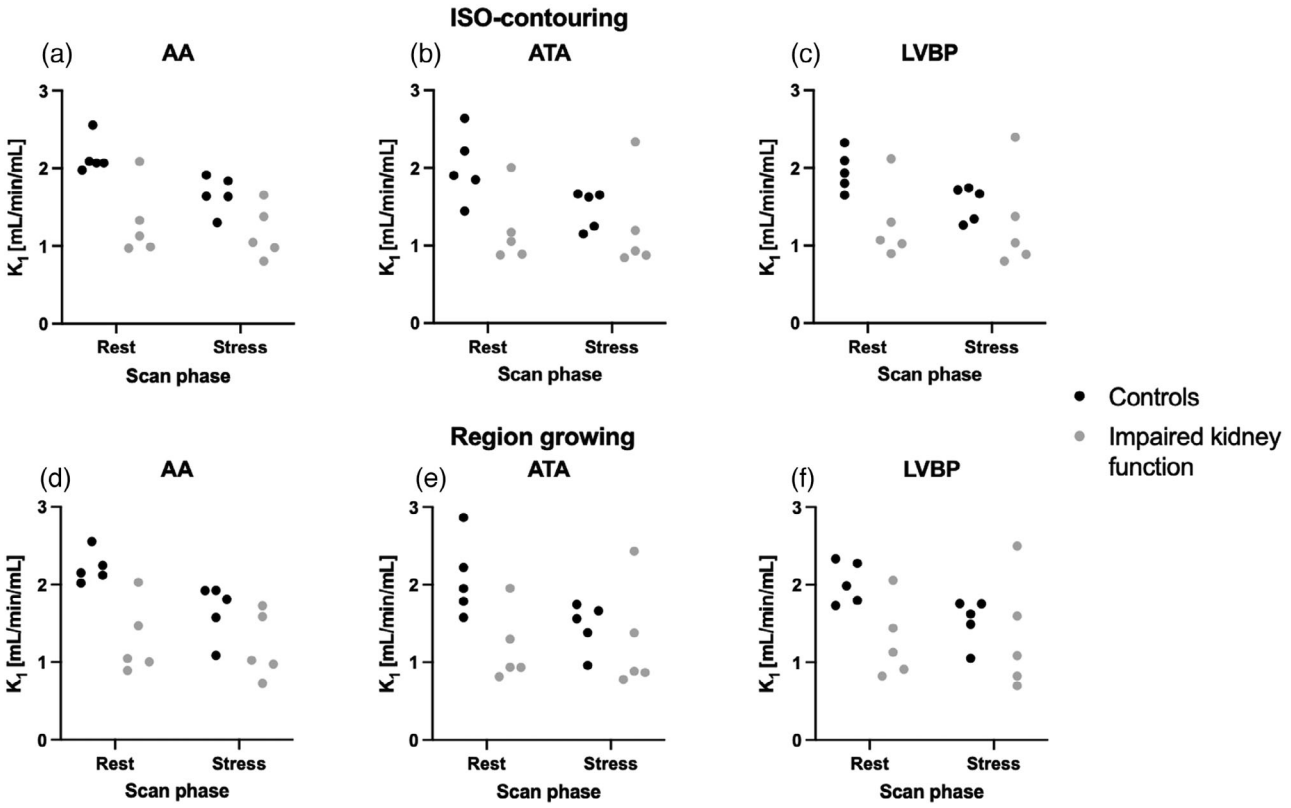

FIGURE 4 K_1 values from a one-tissue compartment model for the abdominal aorta (AA), ascending thoracic aorta (ATA), and left ventricular blood pool (LVBP) as vascular input functions. (a–c) The models obtained by delineation the kidney using iso-contouring and (d–f) using region growing (dataset B, $N = 10$).

were found between the different IDIFs ($p > 0.05$). In the stress phase, significant differences were identified between the LVBP and the ATA for all three flow methods, within the iso-contouring delineation method ($p < 0.05$).

RVR data are presented in Table 1. The control group showed a larger range of values compared to the impaired kidney function group, the latter having median RVR values close to 1.0. The highest median RVR value in the control group was 0.81 (IQR: 0.75–0.82) when a constant extraction combined was applied with iso-contouring and the LVBP as input. The smallest median RVR values were found with flows calculated with Gregg's extraction and the ATA input and were 0.40 (IQR: 0.28–0.66) and 0.40 (IQR: 0.23–0.70) for iso-contouring and region growing, respectively. For the impaired kidney function group, the smallest median RVR value was 0.96 (IQR: 0.62–1.15), calculated with Gregg's extraction fraction. The ATA IDIF yielded significant differences between the control and the impaired kidney function group for both extraction methods and both kidney delineation methods ($p < 0.05$). RVR calculated using Gregg's method resulted in significant differences in all VOIs except for the AA obtained using region growing.

3.4 | Intraobserver variability

Repeated intraobserver measurement data are illustrated in Figure 5. Bland–Altman analysis of the repeated measurements showed smaller agreement intervals for the iso-contouring delineation method, irrespectively of the extraction method. The smallest 95% agreement interval was found for the constant extraction fraction and region growing delineation (−0.2011–0.1857), while the largest interval was found for Gregg's extraction fraction in combination with the region growing delineation method (−0.6254–0.5945). Bias and agreement intervals from the Bland–Altman analysis of RVR values measurements are demonstrated in Table S5.

4 | DISCUSSION

This study represents a unique exploration into the potential utilization of dynamic ^{82}Rb PET/CT for assessing renal perfusion. Various inputs, outputs, and extraction fractions on the RBFs of an existing one-tissue compartment model were evaluated to explore the potential clinical application of ^{82}Rb PET/CT for

TABLE 1 Renovascular reserve (RVR) values as the ratio of renal blood flow in during adenosine (stress) compared to renal blood flow (RBF) in rest.

Adenosine renovascular reserve values				
Flow method	**VOIs**	**Control**	**Impaired kidney function**	***p***
Constant	AA			
	ISO	0.79 (0.75–0.83)	0.99 (0.79–1.04)	0.251
	RG	0.75 (0.70–0.84)	0.98 (0.85–1.08)	0.076
	ATA			
	ISO	0.74 (0.62–0.86)	1.02 (0.96–1.05)	**0.028**
	RG	0.75 (0.55–0.88)	1.06 (0.95–1.07)	**0.028**
	LVBP			
	ISO	0.81 (0.75–0.82)	0.99 (0.97–1.06)	**0.047**
	RG	0.75 (0.71–0.83)	1.00 (0.96–1.11)	**0.028**
Gregg	AA			
	ISO	0.48 (0.43–0.55)	0.98 (0.57–1.09)	0.076
	RG	0.44 (0.33–0.58)	0.96 (0.62–1.15)	**0.028**
	ATA			
	ISO	0.40 (0.28–0.66)	1.04 (0.95–1.08)	**0.009**
	RG	0.40 (0.23–0.70)	1.10 (0.92–1.15)	**0.009**
	LVBP			
	ISO	0.53 (0.41–0.57)	0.98 (0.94–1.14)	**0.009**
	RG	0.41 (0.35–0.57)	1.00 (0.92–1.33)	**0.009**

RVR values were obtained of dataset B ($N = 10$) with various image-derived input functions (IDIFs) derived from abdominal aorta (AA), ascending thoracic aorta (ATA), and left ventricular blood pool (LVBP), two kidney volume of interest (VOI) methods (iso-contouring [ISO] and region growing [RG]), and two extraction methods (constant and Gregg). Values are displayed as median (interquartile range).

assessing renal perfusion. First, K_1 values were generated with various CT-based kidney VOIs between the medulla and the cortex (dataset A). Subsequently, myocardial perfusion data were analyzed retrospectively to obtain renal perfusion measurements in rest and when exposed to adenosine (stress) using various PET-based delineation methods, IDIFS and extraction fractions (dataset B). The RVR for the controls were overall significantly lower ($p < 0.05$) compared to the impaired kidney function group indicating the possibility of measuring differences in kidney hemodynamics with ^{82}Rb PET/CT.

For practical reasons in subsequent analysis one single large VOI was used, even though composing K_1 values for various numbers of CT-based kidney VOI delineations seemed feasible. Literature on kinetic modeling from other fields suggest that larger VOI reduces variation, which supports the use of one kidney VOI to illustrate the clinical applicability.[31,32] Furthermore, VOI delineation was performed on unenhanced CT data obtained for attenuation purposes only (as part of the myocardial perfusion protocol for ischemia detection), limiting the ability to distinguish renal cortex and medulla. Therefore, two other PET-based kidney delineation methods were explored in the remainder of the study using dataset B.

Applying manual CT-based kidney delineations on dataset A, no significant differences were found between the total mean K_1 values of one, two, three, and four kidney VOI placements, indicating that the mean K_1 values were independent of the number of VOI placements. However, significant differences in K_1 values between the VOIs were found applying three and four VOIs, which might indicate that distinction between the medulla and cortex was possible. Preclinical studies have shown that the medullary blood flow can be maintained when the cortical blood flow is severely decreased.[3,33] In future studies, it might be worthwhile to incorporate a gradient of more layers between the medulla and cortex (as previously performed in MRI kidney studies[34–36]) that is adjusted to the spatial resolution of PET/CT[3]. However, applying three and four VOIs resulted in a larger SD of the mean K_1 values and outliers compared to the application of one VOI (Figure 3). This K_1 deviation might be a result of partial volume effects or manual VOI CT-delineations, but might also be explained by the heterogeneous retrospective dataset A with potentially diverse physiological renal K_1 values. Hypothetically, smaller VOIs are more affected by the spill-out effect of neighboring tissues, showing less ^{82}Rb uptake of surrounded lower vascularized structures. Therefore, the optimal number of VOI delineations should be further

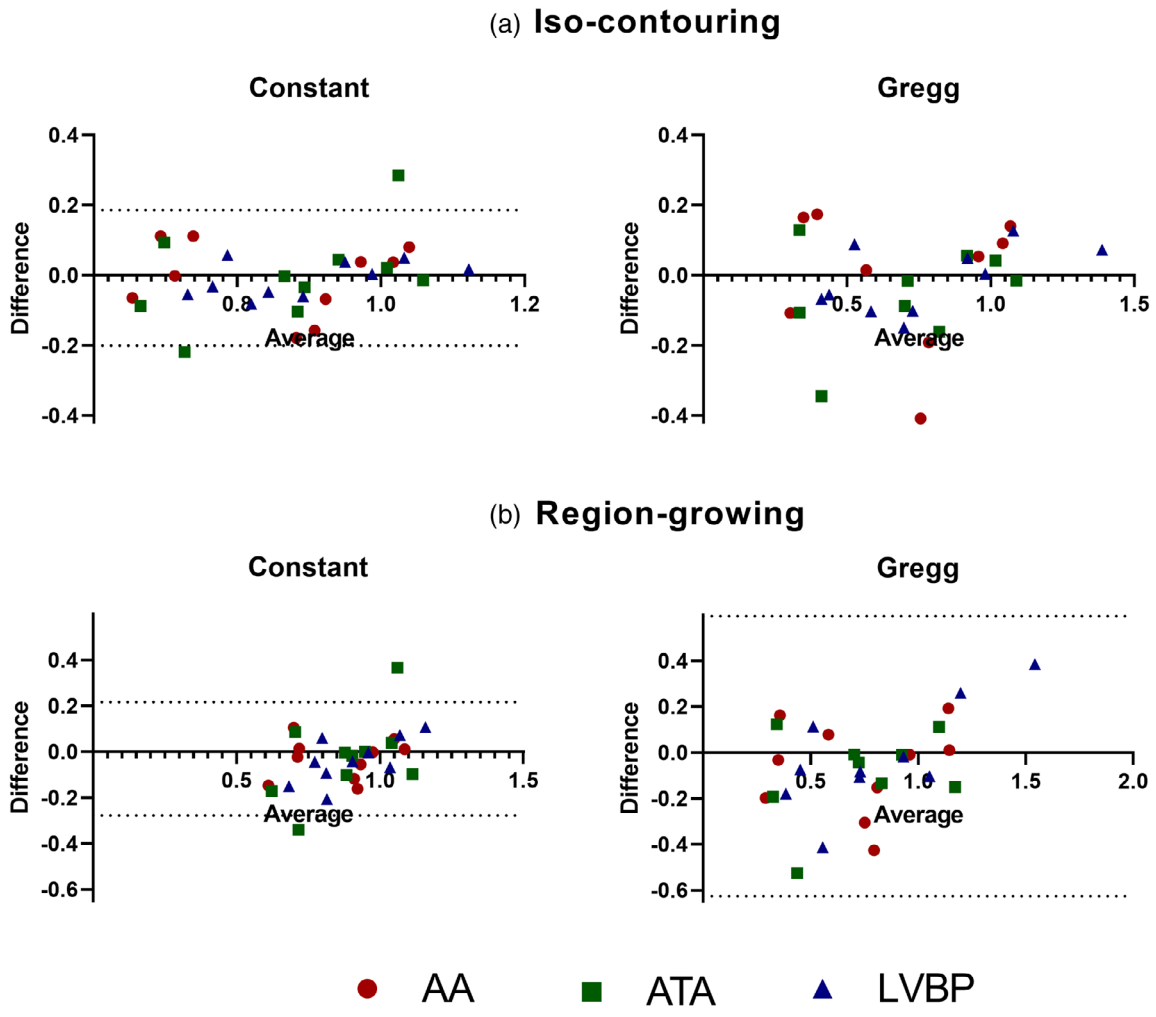

FIGURE 5 Bland–Altman plots of the repeated measurements of the renovascular reserve values: the ratio of renal blood flow during adenosine infusion (stress) compared to renal blood flow in rest. (a) Upper row denotes iso-contouring method and (b) lower row denotes region growing. AA, abdominal aorta; ATA, ascending thoracic aorta; LVBP, left ventricular blood pool.

explored in future studies that are dedicated to applying ^{82}Rb PET/CT to the kidney.

Another possible explanation for the significant differences observed with three and four VOI placements may be attributed to the fixed v_B applied in this study. The value of 0.1 was estimated using the entire kidney of healthy subjects,[13,15] but different VOIs within the kidney might potentially have varying v_B values. However, the objective of our study was to assess the applicability of various kidney VOIs, IDIFs and extraction fractions of a one-tissue compartment model. To achieve this, we extensively reviewed available literature and applied that in our study. Unfortunately, literature regarding v_B of the kidney and renal perfusion using imaging is currently hardly available. Consequently, further research is necessary to investigate the effects of v_B in patients with impaired kidney function and different parts of the kidney in a larger prospective study.

Reproducibility analysis of two PET-based delineation methods showed smaller agreement interval limits for iso-contouring compared to region growing kidney delineation, indicating that iso-contouring is less sensitive for repetition errors. Possible explanations are manual temporal frame selection and manual VOI adjustments, making region growing more prone for errors compared to iso-contouring (which only requires bounding box around the averaged kidney volume).

No significant difference between the region growing and iso-contouring delineations within the same vascular input was found. The LVBP and AA as IDIFs showed the least spread in the Bland–Altman plots, while the IDIF ATA showed the most outliers. Moreover, no significant differences between the IDIFs AA and LVBP with regards to RBF calculation were observed. The IDIF AA is especially interesting for measuring RVR, as this vessel would be in the scan FoV. Therefore, previous renal studies considered it as a suitable alternative to the LVBP, which we confirm in our study.[12,13] Additionally, a high correlation was found between arterial sampling and AA as IDIF in renal studies.[37] This study supports

the feasibility of the use of the AA as IDIF, possibly combined with an iso-contouring kidney delineation method.

Obtained renal K_1 values in five individuals without cardiovascular or renal disease were in line with previous reported renal K_1 values.[12,13] However, to the best of our knowledge, the function describing the extraction of ^{82}Rb in the kidney and the conversion of K_1 to flow is currently unknown. Literature suggests, with a high first pass extraction, a non-linear relationship between the flow and K_1 due to the retention of ^{82}Rb in tissue and the active transport into cells.[38,39] Gregg et al. reported the relation between K_1 and flow in kidney tissue, showing that the extraction function by Gregg deflects more strongly with increasing flow.[25] Future studies comparing K_1 values obtained using ^{82}Rb as flow tracer with a gold standard reference radiopharmaceutical with a linear extraction such as [^{15}O]H_2O is therefore crucial in order to establish a more robust relationship between K_1 values and flow of ^{82}Rb in renal tissue. Moreover, it is essential to further investigate the extraction of ^{82}Rb in the kidney and the conversion of K_1 to flow before the clinical implementation of ^{82}Rb PET/CT measurements can take place.

Changes in RBF between rest and during exposure to adenosine (stress) led to RVRs below 1.0 for the group consisting of individuals without cardiovascular or renal disease, while the RVRs in the group of kidney patients were around 1.0. This might be a direct consequence of our pragmatic choice to use adenosine and retrospective cardiac data. Adenosine is considered a systemic vasodilator while the spleen is also known to exhibit vasoconstriction after adenosine administration.[40] Previous research showed that adenosine has various effects on the renal perfusion.[25,28,41–43] Ultimately, we need a well-established renal stressor that can also be effectively combined with imaging from logistical and technical perspectives.

This study contains some limitations. First, the limited number of subjects constitutes a major limitation and hence our results should be interpreted carefully. However, little is known about the consequences of the changes in RBF, and ^{82}Rb PET/CT data for renal perfusion imaging are scarce. Moreover, non-invasive imaging techniques for assessing renal are not incorporated in clinical practice guidelines due to the lack of evidence. Although our retrospective proof-of-concept study concerns only a small study population, we believe that our findings exhibit the complexity of assessing RBF and contribute to the knowledge of the application of ^{82}Rb PET/CT for kidney perfusion imaging. Second, the study is retrospective in design and used cardiac ^{82}Rb PET/CT data to evaluate the feasibility to assess renal perfusion. As such, the used scan data in the present study was obtained focused on myocardial ischemia detection, with the heart in the center of the FoV, yielding the highest sensitivity.[21] As a result, some parts of the kidney were imaged at the edge of the FoV with lower sensitivity, leading to poorer image quality for the kidney. In addition, adenosine was used as a pharmacological stress agent; however, this is not the ideal "stress agent" for the kidney compared to infusion of amino acids, dopamine, or an acute protein. Langaa et al. has pioneered the use combining ^{82}Rb PET/CT with infusion of amino acids, demonstrating an increase in RBF in healthy volunteers.[6] Future prospective studies should focus on developing a dedicated kidney protocol for ^{82}Rb PET/CT, where both kidneys are centered in the FoV to evaluate various parts of the kidney, applying a renal stress agent, and further explore kinetic modeling with its inputs, outputs, and extraction fractions to evaluate disease activity and treatment response for CKD.

CKD is recognized as one of the leading causes of death worldwide.[44–46] In early stage CKD, patients are often asymptomatic, leading to a diagnosis in later stages when substantial and irreversible kidney damage has already occurred. Given the asymptomatic nature of early stage CKD, there is a need for a novel diagnostic tool or biomarker to enable early treatment, potentially slowing progression, while being cost effective.[47,48] Current clinically available non-invasive imaging techniques for assessing the kidney function or hemodynamics as renal scintigraphy, CT, magnetic resonance imaging (MRI), and ultrasound have drawbacks including limited resolution, observer dependency, scan duration, limited quantification possibilities, and the use of contrast agents that may induce nephrotoxicity and allergic reactions.[49–51]

The scarcity of evidence demonstrating heightened renal hypoxia in humans is mainly attributed to the absence of non-invasive (imaging) techniques for assessing renal oxygenation and fibrosis.[52] However, changes in renal microcirculation are crucial in the pathophysiological processes of renal disease.[53] Given the limited availability of literature in the field of kidney perfusion and various physiological and anatomical similarities among the perfusion of the heart and the kidneys, we found it worthwhile to investigate whether dynamic ^{82}Rb PET/CT was able to detect differences in renal hemodynamics in stress conditions compared to resting state (RVR). Moreover, the coronary flow reserve has been proven to be of added value and has been used in a routine clinical setting for the detection of myocardial ischemia.[10,54] Therefore, ^{82}Rb PET/CT holds potential relevance as an accessible novel diagnostic tool for the early detection of CKD by assessing renal hemodynamics.

5 | CONCLUSION

In this study, it was demonstrated that obtaining renal K_1 and RBF values using ^{82}Rb PET/CT was feasible using a one-tissue compartment model applying either

CT- or PET-based kidney VOI delineation methods (region growing and iso-contouring), IDIFs (AA, ATA, and LVBP), and Gregg's[25] and constant[7] extraction fractions. Applying iso-contouring as the PET-based VOI of the kidney and using AA as an IDIF is suggested for consideration in further studies. Moreover, it is crucial to further investigate the extraction of ^{82}Rb in the kidney and the conversion of K_1 to flow before the clinical implementation of ^{82}Rb PET/CT measurements can take place. Dynamic ^{82}Rb PET/CT imaging showed significant differences in renal hemodynamics in rest compared to when exposed to adenosine. This indicates that dynamic ^{82}Rb PET/CT has potential to detect differences in renal hemodynamics in stress conditions compared to the resting state, and might be useful as a novel diagnostic tool for assessing renal perfusion.

ACKNOWLEDGMENTS

The authors thank Joyce Rijs, Suus van Loosbroek, Sofie Blankers, Emma Buijsman, Thomas Jansen, and Evy Ligtvoet from the Delft University of Technology, and the nuclear medicine department from Alrijne hospital for their contribution, meaningful discussions, and suggestions. Moreover, Ilona A. Dekkers was supported by the Dutch Science Foundation (ZonMW, VENI: 09150162210040).

CONFLICT OF INTEREST STATEMENT

The authors have no conflicts of interest to disclose.

REFERENCES

1. Bello AK, Levin A, Tonelli M, et al. Assessment of global kidney health care status. *JAMA*. 2017;317(18):1864-1881.
2. Stack AG, Casserly LF, Cronin CJ, et al. Prevalence and variation of Chronic Kidney Disease in the Irish health system: initial findings from the National Kidney Disease Surveillance Programme. *BMC Nephrol*. 2014;15:185.
3. Päivärinta J, Anastasiou IA, Koivuviita N, et al. Renal perfusion, oxygenation and metabolism: the role of imaging. *J Clin Med*. 2023;12(15):5141.
4. Amoabeng KA, Laurila S, Juárez-Orozco LE, et al. The utilization of positron emission tomography in the evaluation of renal health and disease. *Clin Trans Imaging*. 2022;10:59-69.
5. Palsson R, Waikar SS. Renal functional reserve revisited. *Adv Chronic Kidney Dis*. 2018;25(3):e1-e8.
6. Langaa SS, Mose FH, Fynbo CA, Theil J, Bech JN. Reliability of rubidium-82 PET/CT for renal perfusion determination in healthy subjects. *BMC Nephrol*. 2022;23(1):379.
7. Mullani N, Ekas R, Marani S, Kim E, Gould K. Feasibility of measuring first pass extraction and flow with rubidium-82 in the kidneys. *Am J Physiol Imaging*. 1990;5(4):133-140.
8. Koopman M, Koomen G, Krediet R, De Moor E, Hoek F, Arisz L. Circadian rhythm of glomerular filtration rate in normal individuals. *Clin Sci (Lond)*. 1989;77(1):105-111.
9. Eckerbom P, Hansell P, Cox E, et al. Circadian variation in renal blood flow and kidney function in healthy volunteers monitored with noninvasive magnetic resonance imaging. *Am J Physiol Renal Physiol*. 2020;319(6):F966-F978.
10. Ziadi MC. Myocardial flow reserve (MFR) with positron emission tomography (PET)/computed tomography (CT): clinical impact in diagnosis and prognosis. *Cardiovasc Diagn Ther*. 2017;7(2):206-218.
11. Lortie M, Beanlands RS, Yoshinaga K, Klein R, Dasilva JN, DeKemp RA. Quantification of myocardial blood flow with 82Rb dynamic PET imaging. *Eur J Nucl Med Mol Imaging*. 2007;34(11):1765-1774.
12. Tahari AK, Bravo PE, Rahmim A, Bengel FM, Szabo Z. Initial human experience with Rubidium-82 renal PET/CT imaging. *J Med Imaging Radiat Oncol*. 2014;58(1):25-31.
13. Langaa SS, Lauridsen TG, Mose FH, Fynbo CA, Theil J, Bech JN. Estimation of renal perfusion based on measurement of rubidium-82 clearance by PET/CT scanning in healthy subjects. *EJNMMI Phys*. 2021;8(1):43.
14. Levey AS, Coresh J, Balk E, et al. National Kidney Foundation practice guidelines for chronic kidney disease: evaluation, classification, and stratification. *Ann Intern Med*. 2003;139(2):137-147.
15. Effros RM, Lowenstein J, Baldwin DS, Chinard FP. Vascular and extravascular volumes of the kidney of man. *Circ Res*. 1967;20(2):162-173.
16. *PMOD Kinetic Modeling User Manual. English. Version 4.4*. 1996–2022; 2022. https://doc.pmod.com/PDF/PKIN.pdf
17. Maguire RP. In: *PET Pharmacokinetic Course Manual*, Revision 151:fbd666813aaa (jun 22, 2012); Eds. van den Hoff J., Maguire RP; Chapter 4, Dresden, Germany 2013.
18. Baron J, Frackowiak R, Herholz K, et al. Use of PET methods for measurement of cerebral energy metabolism and hemodynamics in cerebrovascular disease. *J Cereb Blood Flow Metab*. 1989;9(6):723-742.
19. Herscovitch P, Markham J, Raichle M. Brain blood flow measured with intravenous H215O.: I. Theory and error analysis. *J Nucl Med*. 1983;24(9):782-789.
20. Meyer E. Simultaneous correction for tracer arrival delay and dispersion in CBF measurements by the H215O autoradiographic method and dynamic PET. *J Nucl Med*. 1989;30(6):1069-1078.
21. Pan T, Einstein SA, Kappadath SC, et al. Performance evaluation of the 5-ring GE discovery MI PET/CT system using the national electrical manufacturers association NU 2–2012 Standard. *Med Phys*. 2019;46(7):3025-3033.
22. Bettinardi V, Castiglioni I, De Bernardi E, Gilardi MC. PET quantification: strategies for partial volume correction. *Clin Trans Imaging*. 2014;2(3):199-218.
23. Renkin EM. Transport of potassium-42 from blood to tissue in isolated mammalian skeletal muscles. *Am J Physiol*. 1959;197:1205-1210.
24. Crone C. The permeability of capillaries in various organs as determined by use of the 'indicator diffusion' method. *Acta Physiol Scand*. 1963;58:292-305.
25. Gregg S, Keramida G, Peters AM. (82) Rb tissue kinetics in humans. *Clin Physiol Funct Imaging*. 2021;41(3):245-252.
26. Staanum PF, Frellsen AF, Olesen ML, Iversen P, Arveschoug AK. Practical kidney dosimetry in peptide receptor radionuclide therapy using [(177)Lu]Lu-DOTATOC and [(177)Lu]Lu-DOTATATE with focus on uncertainty estimates. *EJNMMI Phys*. 2021;8(1):78.
27. Bouchet LG, Bolch WE, Blanco HP, et al. MIRD Pamphlet No 19: absorbed fractions and radionuclide S values for six age-dependent multiregion models of the kidney. *J Nucl Med*. 2003;44(7):1113-1147.
28. Hansen PB, Schnermann J. Vasoconstrictor and vasodilator effects of adenosine in the kidney. *Am J Physiol Renal Physiol*. 2003;285(4):F590-F599.
29. Wierema TK, Houben AJ, Kroon AA, et al. Mechanisms of adenosine-induced renal vasodilatation in hypertensive patients. *J Hypertens*. 2005;23(9):1731-1736.
30. Virtanen P, Gommers R, Oliphant TE, et al. SciPy 1.0: fundamental algorithms for scientific computing in Python. *Nat Methods*. 2020;17(3):261-272.
31. van der Weerdt AP, Klein LJ, Boellaard R, Visser CA, Visser FC, Lammertsma AA. Image-derived input functions for determination of MRGlu in cardiac (18)F-FDG PET scans. *J Nucl Med*. 2001;42(11):1622-1629.

32. de Geus-Oei LF, Visser EP, Krabbe PF, et al. Comparison of image-derived and arterial input functions for estimating the rate of glucose metabolism in therapy-monitoring 18F-FDG PET studies. *J Nucl Med*. 2006;47(6):945-949.
33. Trueta J, Barclay AE. Studies of the renal circulation. *Bristol Med Chir J (1883)*. 1948;65(233):16-18.
34. Pruijm M, Milani B, Pivin E, et al. Reduced cortical oxygenation predicts a progressive decline of renal function in patients with chronic kidney disease. *Kidney Int*. 2018;93(4):932-940.
35. Li LP, Tan H, Thacker JM, et al. Evaluation of renal blood flow in chronic kidney disease using arterial spin labeling perfusion magnetic resonance imaging. *Kidney Int Rep*. 2017;2(1):36-43.
36. Milani B, Ansaloni A, Sousa-Guimaraes S, et al. Reduction of cortical oxygenation in chronic kidney disease: evidence obtained with a new analysis method of blood oxygenation level-dependent magnetic resonance imaging. *Nephrol Dial Transplant*. 2017;32(12):2097-2105.
37. Germano G, Chen BC, Huang SC, Gambhir SS, Hoffman EJ, Phelps ME. Use of the abdominal aorta for arterial input function determination in hepatic and renal PET studies. *J Nucl Med*. 1992;33(4):613-620.
38. Szabo Z, Xia J, Mathews WB, Brown PR. Future direction of renal positron emission tomography. *Semin Nucl Med*. 2006;36(1):36-50.
39. Tamaki N, Rabito CA, Alpert NM, et al. Serial analysis of renal blood flow by positron tomography with rubidium-82. *Am J Physiol*. 1986;251(5 pt 2):H1024-H1030.
40. Manisty C, Ripley DP, Herrey AS, et al. Splenic Switch-off: a tool to assess stress adequacy in adenosine perfusion cardiac MR imaging. *Radiology*. 2015;276(3):732-740.
41. Vallon V, Osswald H. Adenosine receptors and the kidney. *Handb Exp Pharmacol*. 2009(193):443-470.
42. Bidani AK, Polichnowski AJ, Loutzenhiser R, Griffin KA. Renal microvascular dysfunction, hypertension and CKD progression. *Curr Opin Nephrol Hypertens*. 2013;22(1):1-9.
43. Oyarzun C, Garrido W, Alarcon S, et al. Adenosine contribution to normal renal physiology and chronic kidney disease. *Mol Aspects Med*. 2017;55:75-89.
44. Jager KJ, Kovesdy C, Langham R, Rosenberg M, Jha V, Zoccali C. A single number for advocacy and communication-worldwide more than 850 million individuals have kidney diseases. *Kidney Int*. 2019;96(5):1048-1050.
45. Kovesdy CP. Epidemiology of chronic kidney disease: an update 2022. *Kidney Int Suppl (2011)*. 2022;12(1):7-11.
46. Tonelli M, Wiebe N, Culleton B, et al. Chronic kidney disease and mortality risk: a systematic review. *J Am Soc Nephrol*. 2006;17(7):2034-2047.
47. Black C, Sharma P, Scotland G, et al. Early referral strategies for management of people with markers of renal disease: a systematic review of the evidence of clinical effectiveness, cost-effectiveness and economic analysis. *Health Technol Assess*. 2010;14(21):1-184.
48. Tonelli M, Dickinson JA. Early detection of CKD: implications for low-income, middle-income, and high-income countries. *J Am Soc Nephrol*. 2020;31(9):1931-1940.
49. Andreucci M, Solomon R, Tasanarong A. Side effects of radiographic contrast media: pathogenesis, risk factors, and prevention. *Biomed Res Int*. 2014;2014:741018.
50. Rydahl C, Thomsen HS, Marckmann P. High prevalence of nephrogenic systemic fibrosis in chronic renal failure patients exposed to gadodiamide, a gadolinium-containing magnetic resonance contrast agent. *Invest Radiol*. 2008;43(2):141-144.
51. Kishimoto N, Mori Y, Nishiue T, et al. Ultrasound evaluation of valsartan therapy for renal cortical perfusion. *Hypertens Res*. 2004;27(5):345-349.
52. Fine LG, Norman JT. Chronic hypoxia as a mechanism of progression of chronic kidney diseases: from hypothesis to novel therapeutics. *Kidney Int*. 2008;74(7):867-872.
53. Alhummiany B, Sharma K, Buckley DL, Soe KK, Sourbron SP. Physiological confounders of renal blood flow measurement. *Magn Reson Mater Phys, Biol Med*. 2023:1-18.
54. Ziadi MC, Dekemp RA, Williams KA, et al. Impaired myocardial flow reserve on rubidium-82 positron emission tomography imaging predicts adverse outcomes in patients assessed for myocardial ischemia. *J Am Coll Cardiol*. 2011;58(7):740-748.

SUPPORTING INFORMATION

Additional supporting information can be found online in the Supporting Information section at the end of this article.

How to cite this article: van de Burgt A, van Velden FHP, Kwakkenbos K, Smit F, de Geus-Oei L-F, Dekkers IA. Dynamic rubidium-82 PET/CT as a novel tool for quantifying hemodynamic differences in renal blood flow using a one-tissue compartment model. *Med Phys*. 2024;51:4069–4080. https://doi.org/10.1002/mp.17080